Int. J. Cancer: **123,** 464–475 (2008)

Tumoricidal activity of high-dose tumor necrosis factor-α is mediated by macrophage-derived nitric oxide burst and permanent blood flow shutdown

Chandrakala Menon[1]*, Todd W. Bauer[1], Scott T. Kelley[1], Dan J. Raz[1], Joshua I. Bleier[1], Krina Patel[1], Kirsten Steele[1], Indira Prabakaran[1], Alexander Shifrin[1], Donald G. Buerk[2], Chandra M. Sehgal[3] and Douglas L. Fraker[1]

[1]*Department of Surgery, University of Pennsylvania, Philadelphia, PA*
[2]*Department of Physiology, University of Pennsylvania, Philadelphia, PA*
[3]*Department of Radiology, University of Pennsylvania, Philadelphia, PA*

This study investigates the role of tumor nitric oxide (NO) and vascular regulation in tumor ulceration following high-dose tumor necrosis factor-α (TNF) treatment. Using TNF-responsive (MethA) and nonresponsive (LL2) mouse tumors, tumor NO concentration was measured with an electrochemical sensor and tumor blood flow by Doppler ultrasound. Mice were also pretreated with a selective inducible nitric oxide synthase (iNOS) inhibitor, 1400 W. Tumors harvested from TNF-treated mice were cryosectioned and immunostained for murine macrophages, or/and iNOS. MethA tumor-bearing mice were depleted of macrophages. Pre- and post-TNF tumor NO levels were measured continuously, and mice were followed for gross tumor response. In MethA tumors, TNF caused a 96% response rate, and tumor NO concentration doubled. Tumor blood flow decreased to 3% of baseline by 4 hr and was sustained at 24 hr and 10 days post-TNF. Selective NO inhibition with 1400 W blocked NO rise and decreased response rate to 38%. MethA tumors showed tumor infiltration by macrophages post-TNF and the pattern of macrophage immunostaining overlapped with iNOS immunostaining. Depletion of macrophages inhibited tumor NO increase and response to TNF. LL2 tumors had a 0% response rate to TNF and exhibited no change in NO concentration. Blood flow decreased to 2% of baseline by 4 hr, recovered to 56% by 24 hr and increased to 232% by 10 days. LL2 tumors showed no infiltration by macrophages post-TNF. We conclude that TNF causes tumor infiltrating, macrophage-derived iNOS-mediated tumor NO rise and sustained tumor blood flow shutdown, resulting in tumor ulceration in the responsive tumor.

Key words: high-dose TNF; nitric oxide; blood flow; macrophage; tumor

The therapeutic potential of targeting the tumor vascular supply is now widely recognized and has led to improvement in survival in patients with advanced cancer.[1–3] Continued investigation into novel strategies of antivascular therapies and further study of the mechanisms of current antivascular therapies will help to advance this field.

Regional perfusion with high-dose recombinant human tumor necrosis factor-α (TNF) is an effective antivascular therapy in clinical practice. It achieves an overall response rate of 90–100% and complete response rate of 80–90% when combined with melphalan for extremity melanoma, making this treatment one of the most effective single-administration therapies for solid malignancies.[4–6] TNF in combination with melphalan has demonstrated synergistic antitumor activity in the treatment of melanomas and soft tissue sarcomas that are recurrent, deep-seated or bulky. One of the advantages of this therapeutic is that it is selective to tumor tissue and spares surrounding normal tissue.[7] Despite the tumoricidal potential of TNF, severe toxicity such as hypotension, abnormalities in liver function, leukopenia and thrombus formation has made TNF difficult to be used systemically as an antitumor drug. This problem has been circumvented by using isolated limb perfusion (ILP) technique in human patients who have unresectable extremity-limited in-transit metastatic disease.[8,9] Success of this regimen has also been reported for multifocal skin cancers and drug-resistant bony sarcomas.[10] ILP treatment is based on the ability to isolate the circulation of the afflicted extremity from systemic circulation, thereby allowing dose-intensive delivery of anticancer agents to the limb while eliminating systemic exposure and toxicity.[11] ILP treatment with TNF plus melphalan can avoid the need for limb amputation in extremity-limited melanoma and sarcoma patients of all ages, especially in older patients.[12] This treatment regimen has also been used as a palliative treatment in selected stage IV melanoma patients with symptomatic advanced limb disease.[13] This combination therapy has also found use in the treatment of a single organ disease as in the case of isolated hepatic perfusion to treat hepatic malignancies that constitute the life-limiting component of disease secondary to colorectal cancer, ocular melanoma, neuroendocrine tumors as well as primary colangio- or hepatocellular carcinomas.[14] In Europe, TNF is approved for regional therapy of soft tissue sarcoma. Further investigation into the mechanism of the antivascular effect of TNF will broaden our understanding of vascular-targeted therapies.

Tumor necrosis and regression by TNF is believed to be mediated by a specific antivascular effect.[15–18] Manda *et al.*[15] demonstrated necrosis of MethA tumors grown intradermally in mice if TNF was given on Days 7 or 10, when tumors have an established vasculature, but not on Day 3. Additionally, TNF had no cytotoxic effect on the MethA cells *in vitro*. These 2 findings support the hypothesis that TNF is primarily targeting tumor vasculature, rather than causing direct tumor cytotoxicity. The antivascular effect of TNF was studied by Nawroth *et al.*,[16] who observed an 80% reduction in tumor blood flow and intravascular fibrin formation following TNF injection in MethA fibrosarcomas. Watanabe *et al.*[17] showed vascular congestion in MethA tumors 4–6 hr after TNF injection, and blood flow shutdown at 24 hr and noted that suppression of the thrombus formation with heparin had no effect on the necrotic response. Thus, TNF appears to decrease tumor blood flow independent of thrombus formation. Additionally, TNF has been shown to stimulate NO production in vascular smooth muscle cells,[19,20] endothelial cells,[21,22] and macrophages,[23,24] and high NO levels have been shown to cause tumor regression.[25–31]

The precise role that NO plays in the antivascular effect of TNF has not been fully described. We used a murine tumor model system consisting of MethA fibrosarcoma (TNF-sensitive tumor) and Lewis lung carcinoma (TNF-resistant tumor), with systemic TNF administration to investigate the role of tumor blood flow shutdown and nitric oxide (NO) elevation on tumor regression. We used an inhibitor to further study the role of inducible nitric oxide synthase (iNOS) in tumor blood flow and tumor NO elevation following TNF administration. The present work also attempts to delineate the cell-type source of the NO burst post-TNF in the TNF-responsive MethA tumor type. This work introduces the possibility that although TNF may primarily express its antitumor activity *via* an antivascular mechanism, there could likely be a secondary component that causes tumor cell kill *via* a selective tumor

---

The first two authors contributed equally to this work.

Grant sponsor: Georgene S. Harmelin Endowment Fund.

***Correspondence to:** 927 Blockley Hall, 423 Guardian Drive, University of Pennsylvania, Philadelphia, PA 19104, USA. Fax: +215-614-0765. E-mail: menonc@uphs.upenn.edu

Received 24 May 2007; Accepted after revision 10 January 2008
DOI 10.1002/ijc.23499
Published online 30 April 2008 in Wiley InterScience (www.interscience.wiley.com).

infiltrating macrophage-mediated pathway. Tumor-infiltrating macrophages and the free radical NO produced by these macrophages in response to TNF treatment appear to be common intermediates in both the antivascular as well as direct tumor cell kill pathways. Furthermore, the present work attempts to delineate the mechanism underlying the differential tumor response to TNF as represented by the TNF-sensitive MethA fibrosarcoma and the TNF-resistant LL2 tumor types.

Material and methods

Animals

Female BALB/c and C57BL/6 mice (Taconic, Germantown, NY) aged 5–7 weeks, weighing 18–22 g, were housed in the University of Pennsylvania Animal Facility under standard light and accommodation conditions and fed a standard laboratory diet. The experimental protocol was approved by the University of Pennsylvania Institutional Animal Care and Use Committee.

Tumor cell lines

MethA murine fibrosarcoma cells (obtained from Steven Rosenberg, National Cancer Institute, Bethesda, MD) were grown as a monolayer in Roswell Park Memorial Institute (RPMI) medium (GibcoBRL, Green Island, NY) supplemented with 10% (v/v) fetal calf serum (FCS; HyClone, Logan, UT), L-glutamine, penicillin G, streptomycin, amphotericin and gentamycin. LL2 murine Lewis lung carcinoma cells (obtained from Steven Rosenberg) were grown as a monolayer in Dulbecco's modified eagle's medium (DMEM, GibcoBRL) supplemented with 10% (v/v) FCS, L-glutamine, penicillin G, streptomycin, amphotericin and gentamycin. Exponentially growing cultures of MethA and LL2 were maintained in a humidified atmosphere of 5% CO_2–95% air at 37°C and were tested every 6 months for mycoplasma.

Tumor inoculation and measurement

A chemical depilatory (Nair, Carter Wallace, New York, NY) was applied to the right flank of the mice 24–48 hr prior to tumor inoculation. BALB/c mice were injected subcutaneously in the right flank with 1×10^6 MethA cells, and C57BL/6 mice were similarly injected with LL2 cells. The tumors and tumor ulcer were measured in 2 perpendicular dimensions, and tumor volume was calculated using the formula $v = [1/2]\ ab^2 - [1/2]\ cd^2$, where v is the tumor volume, a the tumor length, b the tumor width, c the ulcer length and d is the ulcer width. A response to treatment was defined as $\geq$25% decrease in tumor volume, or gross ulceration of the tumor plus $\geq$12.5% decrease in tumor volume.

TNF and NOS inhibitor administration

When the tumors grew to a maximal dimension of 10 mm, the mice were injected by tail vein with 15 μg TNF (Knoll Pharmaceuticals Co., Whippany, NJ) in 0.5 ml 0.5% bovine serum albumin (BSA, Calbiochem, LaJolla, CA). The bioactivity of the TNF was measured by the standard 3-(4,5-dimethylthiazol-2-yl)-2,5-diphenyltetrazolium bromide (MTT) bioassay,[32] and the 15 μg dose was equivalent to 3.3×10^4 U. The selective[33] iNOS inhibitor, 1400 W (Alexis Corp., San Diego, CA) at a dose of 5 mg/kg (0.01 mg/ml) in PBS (Product 14040-117, Invitrogen Corp., Carlsbad, CA), was administered subcutaneously in the left (nontumored) flank.

NO measurements

The tumor NO concentrations were obtained by direct *in vivo* electrochemical measurements using Nafion polymer-coated gold NO microsensors.[34] The NO microsensors were fabricated from gold-plated metal-filled glass micropipettes, with tip diameters between 5 and 15 μm and recessed 50 μm deep. The NO microsensors were calibrated in 0.9% NaCl equilibrated with 100% N_2 (zero NO) and 1,800 ppm NO (balanced N_2) at 37°C before and after each experiment. Typical current sensitivities range between 0.5 and 5 picoampere/micromole NO, depending on tip diameter and recess depth.

The mice were anesthetized with ketamine (Abbott Laboratories, N. Chicago, IL) 2.5 mg i.p. and xylazine (Xyla-ject, Phoenix Pharmaceuticals, St. Joseph, MO) 0.19 mg i.p. and placed on a 37°C warming blanket. The skin ~3–4 mm from the tumor was sutured loosely to a stainless steel ring support to gently elevate the tumor off the body wall to eliminate movement of the tumor with respiration (this was necessary to prevent the delicate microsensor from breaking with respiratory movement). A 2-mm longitudinal incision was made in the skin overlying the tumor (this was necessary to prevent the microprobe from breaking upon insertion). The microprobe was inserted into the middle of the tumor and remained fixed in this location for the duration of the experiment. The tumor surface was superfused with 37°C 0.9% NaCl solution. Polarographic currents at the oxidation potential for NO (+850 mV) were measured with the microsensor relative to a grounded Ag/AgCl reference electrode in contact with the tumor and superfusion bath. All signals were acquired by computer with 12-bit resolution at 1-Hz sampling rates. The NO signal was low-pass filtered through an analog circuit with a 5-Hz cutoff.

NO measurements were obtained for 15–20 min to obtain a stable baseline prior to NOS inhibitor and TNF administration. Following TNF administration, the tumor NO concentration was measured for 1.5–4.5 hr. The mice were allowed to recover from anesthesia, and the tumors were measured with calipers for 14 days.

Blood flow, blood volume and perfusion measurements

Tumor blood flow and blood volume were measured using sonographic imaging in power Doppler (PD) and color Doppler (CD) modes, respectively. This was performed using an L10-5 MHz transducer and an HDI 5000 scanner (Philips Medical Systems, Bothell, WA) as previously described by Sehgal *et al*.[35,36] Ten cross-sectional images in 2 perpendicular planes for PD and CD mode were recorded digitally for each mouse at baseline prior to TNF, then at 4 hr, 24 hr and 10 days. The settings used for PD were as follows—color map: 1; wall filter: medium; gain: 80. The settings used for CD were as follows—color map: 1,4; wall filter: medium; PRF: 1,000; gain: 78; velocity scale: 6.4. All of the imaging parameters were kept constant throughout the study.

To visualize tumor tissue perfusion, the bisbenzamide fluorescent dye, Hoechst 33342 (H33342, Molecular Probes, Eugene, OR) was injected i.v. at different times after TNF, and tumors were then harvested 3 min later for cryosectioning and imaging. This DNA-binding dye fluoresces blue under ultraviolet light. It is rapidly removed from the circulation with a half-life of 2 min,[37] diffuses into cells and binds specifically and quantitatively to DNA.[38] The degree of blue fluorescence in the tumor is a measure of tissue perfusion. MethA tumors were harvested at 30, 45, 60, 90, 120, and 180 min after TNF. Hoechst dye was injected at a dose of 11.2 mg/kg (5.6 mg/ml in distilled water) i.v., 3 min before tumor harvest. Tumors were harvested, frozen in OCT, cryosectioned and photographed as described later. Sections were then stored at −20°C.

CD31 immunohistochemistry

Serial tissue sections (adjacent to those used for perfusion analysis with Hoechst dye) were stained for CD31 to evaluate vessel architecture of the tumors in relation to the tissue perfusion visualized by Hoechst dye. Sections were fixed in cold 4% paraformaldehyde for 1 hr, rinsed in PBS, blocked overnight in PBS containing 1.5% BSA and 0.3% Tween 20 [(ttPBS) Product X251-07, J.T. Baker, Phillipsburg, NJ] supplemented with 5% skim milk and 5% normal mouse serum. The slides were then incubated with a 1:100 dilution of rat anti-mouse CD31 monoclonal antibody IgG2a,κ (MEC 13.3, PharMingen, San Diego, CA) overnight at 4°C in a humid box. The slides were rinsed 3 times in ttPBS for 15 min. The ttPBS was blotted off, and the slides were incubated

with Cy5-conjugated affinipure mouse anti-rat IgG (Jackson ImmunoResearch, West Grove, PA). The slides were then rinsed with ttPBS and viewed and photomicrographed as described later.

Imaging of Hoechst dye and CD31

A Nikon Lab-Photofluorescence microscope equipped with a 100-W high pressure mercury arc lamp, a cooled (−25°C) charge-coupled device camera (Quantix by Photometric, Tucson, AZ), and an automatic stage advancement (Ludl Electronic Products, Hawthorne, NY) was used. Digital control of the camera and stage was provided by a Macintosh 9600 Power PC running IPLab Spectrum software (Scanalytics, Fairfax, VA). Images of each tissue section were collected as several individual images, and composites were made with IPLab Spectrum software. Field flattening was performed by subtraction of an image of an empty field acquired with the same exposure as for the section of interest. Epi-illumination images of the fluorescent blue Hoechst staining were obtained immediately after the 4.0-μM sections were made. UV excitation was at 330–380 nm, with a 400-nm dichroic and a 420-nm barrier filter (UV-2A filter cube), and care was taken to avoid both normal tissue and sectioning artifacts. After CD31 staining was completed, the same tumor section used for the Hoechst imaging was returned to the microscope stage and automatically rescanned using the same coordinates as for the initial composite images. Matching composite images of the CD31 staining were acquired. The Hoechst and CD31 images were then superimposed using the IPLab Spectrum software.

Immunohistochemistry for iNOS

MethA and LL2 tumors from TNF or BSA-treated anesthetized mice were harvested at 30 min, 1, 2, 4, 8, 16 and 24 hr after treatment, frozen in OCT (Tissue-Tek, Sakura Finetek USA, Torrance, CA) and cryosectioned into 5-μm sections. The tumor tissue sections were fixed in cold acetone for 5 min, air-dried and treated with 0.3% H_2O_2 for 5 min to quench endogenous peroxides. The tissue sections were rinsed in 1× PBS for 3 × 5 min and were blocked in blocking buffer consisting of 1% BSA and 5% horse serum in 1× PBS for 1 hr. The slides were incubated with a 3:100 solution of goat anti-mouse polyclonal iNOS antibody (Santa Cruz Biotechnology, Santa Cruz, CA) in blocking buffer and left at room temperature for 1 hr. The slides were rinsed in 1× PBS for 3 × 5 min and then incubated with a 1:50 solution of biotinylated horse anti-goat IgG (H+L) secondary antibody (Vector Labs, Burlingame, CA) in blocking buffer for 1 hr. The slides were again rinsed 3 × 5 min in 1× PBS. Color development was carried out using the Vector ABC Elite® kit and the Vector AEC® peroxidase substrate kit. The slides were mounted using glycerol and photomicrographed at 200× under a bright-field microscope.

Immunohistochemistry for tumor-infiltrating macrophages

MethA and LL2 tumor cryosections from 1, 2, 4, 8, 16 and 24 hr post-TNF or BSA treatment were fixed in cold acetone for 5 min, air-dried and treated with 0.3% H_2O_2 for 5 min to quench endogenous peroxides. The tissue sections were rinsed in 1× PBS for 3 × 5 min and were blocked in blocking buffer consisting of 1% BSA and 5% rabbit serum in 1× PBS for 1 h. Control slides were left in blocking buffer, and the remaining slides were incubated with a 3:100 solution of rat anti-mouse F4/80 primary antibody (BD Biosciences, San Diego, CA) in blocking buffer and left at room temperature for 1 hr. The slides were rinsed in 1× PBS for 3 × 5 min and then incubated with a 1:50 solution of biotinylated rabbit anti-rat IgG (H+L) mouse adsorbed secondary antibody (Vector Labs) in blocking buffer for 1 hr. The slides were again rinsed 3 × 5 min in 1× PBS. Color development was carried out using the Vector ABC Elite kit and the Vector SG peroxidase substrate kit. The slides were mounted using glycerol and photomicrographed at 200× using a bright-field microscope.

Double-immunohistochemical labeling for tumor-infiltrating macrophages and iNOS expression

TNF- or BSA-treated MethA and LL2 tumor cryosections from 1, 2 and 4 hr posttreatment were processed as described earlier for immunostaining of tumor infiltrating macrophages, using the primary and secondary antibodies listed earlier. The slides were then blocked with blocking buffer consisting of 1% BSA and 5% horse serum in 1× PBS for 1 hr, and the slides were processed as described earlier for immunostaining for iNOS. The slides were again rinsed 3 × 5 min in 1× PBS, mounted using glycerol and photomicrographed at 200× under bright-field microscopy.

Preparation of clodronate-containing liposomes

Seventy-five milligrams of phosphatidylcholine (egg lecithin; Sigma, St. Louis, MO) and 19 mg of cholesterol (Sigma) were dissolved in 5 ml of chloroform (Fisher Scientific, Pittsburgh, PA) in a 250-ml round-bottomed flask. The chloroform phase was removed by evaporation at room temperature for 2–4 hr (or overnight) under low vacuum (200–150 mbar) and at 1,500 rpm rotation, until a thin milky white phospholipid film formed against the inner wall of the flask. The phospholipid film was dispersed in 10 ml PBS containing 1.89 g clodronate (Sigma). The milky white suspension was kept at room temperature for 2 hr under nitrogen gas, and after gentle shaking of the suspension was sonicated in a water bath sonicator for 3 min. The suspension was again kept under nitrogen gas for 2 hr at room temperature to allow for swelling of liposomes. The liposome-containing emulsion was centrifuged at 10,000*g* for 15 min to remove nonencapsulated clodronate. The clodronate-containing liposomes formed a white band at the top of the suspension and was separated from the remaining clear solution by using a syringe to remove the clear fluid from under the clodronate–liposome layer. The clodronate–liposomes were washed 2–3 times using sterile PBS and centrifuged at 25,000*g* for 30 min each, to recover them. The final pellet was resuspended in 4 ml of sterile PBS and stored at 4°C under nitrogen gas for up to 2 weeks, until they were ready to be used for *in vivo* macrophage depletion.

Macrophage depletion in mice

BALB/c mice were either given 25 mg of silica (Sigma) in 100 μl PBS or 100 μl liposomes containing clodronate by i.p. injections 24 hr before TNF treatment. Macrophage depletion was confirmed by immunohistochemistry for macrophages in spleen and liver and tumor cryosections from depleted and nondepleted mice at 4 days postdepletion.

In vitro *tumor cell cytotoxicity assay with TNF-treated macrophages*

Isolation of macrophages from BALB/c mice. Five BALB/c mice, 7- to 8-week-old, (Taconic, Hudson, NY) were injected intraperitoneally with 1 ml of 3% thioglycollate broth. After 5 days, peritoneal macrophages were harvested and plated in 96-well plates for 3 hr at 5 × 10^5 cells/well. Half the wells were then exposed to 2 μg/ml TNF in a final volume of 200 μl/well for 20–24 hr before harvest. The harvested "activated" macrophages were washed to remove excess TNF and directly used in the cell lysis assay.

Radiolabeling of MethA cells. MethA tumor cells were radiolabeled by adding 200 μCi (in 200 μl) of tritiated thymidine to culture media in flasks, and the cells were incubated overnight. Tumor cells were collected from the flasks, rinsed twice with RPMI medium, centrifuged at 1,000 rpm and resuspended at a density of 5 × 10^4 cells/ml. Radiolabeled MethA cells were added to the wells containing macrophages at a density of 1 × 10^4 cells/well. Tumor cells that were plated without macrophages were used as controls. After an incubation period of 24 hr, the cells were spun in the 96-well plate at 1,000 rpm. To 3 of the tumor cell-alone containing wells, 22 μl of 10% SDS solution was added to give total cell lysis values. Radioactivity in 100 μl (111 μl from total

cell lysis wells) of supernatant from each well was read in a scintillation counter. Results were expressed as percentage of total cell lysis.

MTT assay on tumor cells after 24-hr SNAP incubation

Single cell suspensions of MethA and LL2 cells were added to 96-well culture plates at 10^5 cells/well. After 16–24 hr incubation at 37°C, cells were exposed to varying concentrations of the NO donor, *S*-nitroso-*N*-acetyl-penicillamine (SNAP; Calbiochem, San Diego, CA), in 100 μl of serum-free medium, regular medium or tumor conditioned medium. The medium was then siphoned out, 50 μl of 2 mg/ml MTT was added to each well and incubated for 4 hr at 37°C. Plates were inverted to remove the MTT solution and 100 μl of DMSO was added to each well. The plates were placed on a shaker for 15 min. Absorbance was read at 490 nm in a scanning multiwell spectrophotometer. Absorbance readings were normalized and treatment values were divided by negative control values × 100 to calculate percent viable cells remaining.

Chemotaxis assay: Monocyte extraction from Balb/c mice. Blood was drawn from the tails of Balb/c mice in a syringe containing the anticoagulant, phosphate–dextrose–adenosine. Blood was diluted 1:1 or 1:2 with Hank's buffered salt solution (HBSS) depending on the viscosity of the drawn blood. An equal volume of the lymphocyte separation medium, Ficoll-hypaque (Sigma Aldrich, St. Louis, MO) was layered under the blood using a Pasteur pipette. The solution was spun at 400*g* for 30 min at 25°C. After centrifugation, the top layer was discarded, and a 2-ml pipette was used to draw the filmy "buffy coat" containing leukocytes. This layer was rinsed with HBSS, spun at 400 *g* and resuspended in 10 ml of RPMI medium. The cells were plated on to a Petri dish at 37°C and incubated for 40 min. The supernatant was discarded, and the adherent cells were replenished with 10 ml of HBSS. When ready to use, the adherence of cells was disrupted using a cell scraper, cells were counted under a microscope and resuspended in a stock solution containing about 50,000–100,000 cells/well. A small aliquot was used to check for quality of isolated monocytes by flow cytometry.

Nucleopore chemotaxis chamber (5-μm pore; 3.2 mm/300 μl well; Neuroprobe, Gaithesburg, MD) were used. The bottom wells were filled with 340 μl of one of the following: (*i*) LL2 or MethA-conditioned medium, (*ii*) TNF-exposed LL2 or MethA conditioned medium, (*iii*) fresh RPMI, (*iv*) fresh RPMI plus 2 μg/ml TNF or (*v*) the chemoattractant agent *N*-formyl-Met-Leu-Phe (fMLP) at 1 ng/ml (Sigma), in replicates of 6. TNF-exposed conditioned medium was obtained by adding TNF directly to LL2- and MethA-containing cell-culture flasks to a final concentration of 2 μg/ml, incubating for 1 hr and then isolating the medium by filtering through a 2-μm filter. After solutions were added, the chamber filter was placed over the wells, and 30 μl of a prepared monocyte RPMI solution taken from the stock solution of monocytes isolated in the laboratory from Balb/c mice was added to the top well at a concentration of 1,500–3,000 cells/well. The system was incubated for 3 hr at 37°C and 5% CO_2 and the filter was carefully removed. Cells that had migrated to the bottom wells were manually counted. Representative high-power fields (hpf) were counted for each of 6 replicates per experimental condition. Data were first statistically analyzed for trend by conditioned medium. Differences in mean migration of monocytes between any of the groups were analyzed using 1-way analysis of variance. This was followed by a 1-way analysis of variance using Bonferroni correction for multiple comparisons, to test for specific differences between any 2 groups.

Immunohistochemistry for ICAM, VCAM and E-selectin

Immunohistochemistry using ICAM, VCAM and E-selectin antibodies was used to visualize the location and expression level of the cell-adhesion molecules in the sections of the vasculature of the 2 tumor types, at each time-point. ICAM, VCAM and E-selectin antibodies were purchased from Santa Cruz Biotechnology. All 3 adhesion molecules were affinity-purified goat polyclonal antibodies. The slides were fixed in cold acetone. Following fixing, endogenous peroxidases were quenched using a 0.1% solution of hydrogen peroxide. The sections were blocked with a solution containing 1% BSA and 5% horse serum. The sections were then incubated with a 1:250 dilution of the aforementioned antibodies overnight at 4°C. The slides were rinsed several times in phosphate buffered saline and then incubated with a horse anti-goat secondary antibody. Color reaction was developed using the standard DAB kit (Vector Labs). Appropriate secondary antibody controls were used. The slides were viewed under brightfield microscopy at a magnification of 200×, and photomicrographs were obtained using a digital camera attached to the microscope. The slides were scored by 2 blinded observers for intensity of immunostaining of the respective antigens.

Detection of ICAM and VCAM expression by ELISA

Tumors measuring 8–10 mm were harvested at various timepoints (30 min, 1, 2, and 4 hr) post-TNF injection and were snap-frozen in liquid nitrogen. Tumors were homogenized in lysis buffer (50 mM Tris-HCl pH 7.5, 150 mM NaCl, 1 mM EDTA, 0.5% Triton X-100, and protease inhibitors 1 mM PMSF, 2 μg/ml aprotinin, 2 μg/ml pepstatin, 2 μg/ml leupeptin) on ice and centrifuged at 11,500*g* for 30 min. Supernatant was collected and total protein was quantitated using BCA Protein Assay kit (Pierce, Rockford, IL). ELISA was performed using R&D kit (Minneapolis, MN) per manufacturer's protocol. VCAM and ICAM protein amounts were expressed per mg/total protein of tumor tissue.

Detection of MCP-1 production in tumor cells by ELISA

Approximately 1×10^5 MethA or LL2 cells were plated into a 24-well cell culture plate in 500 μl of DMEM medium. The next day, cells were exposed to 0 ng/ml, 2 ng/ml, 20 ng/ml, 200 ng/ml or 2 μg/ml of TNF for 1, 2, 8 or 24 hr. The supernatants were collected and spun down at 5K rpm for 3 min in a microcentrifuge at 2000*g*. Supernatants were stored immediately at −80°C until all supernatants were ready to be analyzed by ELISA as per the protocol for MCP-1 ELISA kit (Pharmingen).

Statistical analyses

Statistical analysis was performed using SigmaStat version 2.03 (SPSS, San Rafael, CA) or Stata version 9 (StataCorp LP, College Station, TX). The average changes in tumor NO were analyzed by Mann–Whitney rank sum test. The effect of NOS inhibition on response rate was compared using Fisher's exact test. Maximal decrease in tumor size and data from *in vitro* macrophage cyotoxicity experiments as well as the monocyte migration experiments were analyzed using the 1-way ANOVA with Bonferroni correction for multiple comparisons. The Student's *t*-test was used to analyze the NO donor, SNAP data in MethA and LL2 cells.

Results

To study the mechanism of the antitumor response to TNF, we used a murine tumor model system with a TNF-responsive tumor (MethA fibrosarcoma) and a TNF-resistant tumor (LL2, Lewis lung carcinoma). LL2 tumors treated with TNF had a 0% response rate and had a relative tumor volume of 1.97 ± 0.12 by Day 4 compared to 2.12 ± 0.25 in the BSA-treated mice (Fig. 1). MethA tumors treated with BSA had a 0% response rate with a relative tumor volume at 4 days of 2.52 ± 0.33 (Fig. 1). Thus, the LL2 and MethA tumors in the control group (BSA) had a similar growth rate, and in LL2, there was no appreciable antitumor effect from TNF compared to control treatment (BSA). MethA tumors treated with TNF had a 96% response rate ($p < 0.001$ *vs.* BSA) with a mean 66 ± 5% decrease in tumor volume with maximal response occurring, on average, at Day 4 (Fig. 1). The MethA group had a relative tumor volume of 0.49 ± 0.06 at Day 4, followed by

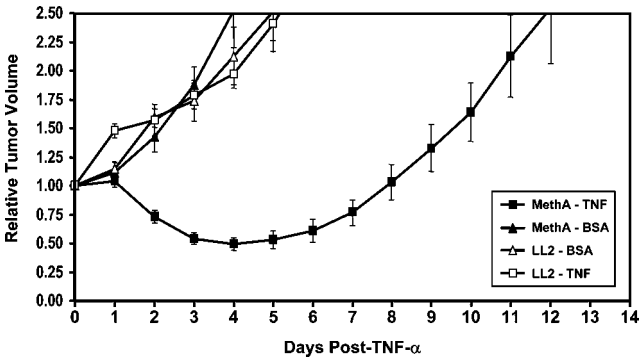

FIGURE 1 – Tumor response following TNF. A single dose of TNF resulted in a significant decrease in MethA tumor volume compared to treatment with BSA. Treatment of LL2 tumors with TNF resulted in increase in tumor volume compared to treatment with BSA. Bars, SE.

regrowth in 21 of 28 (75%), whereas the remaining 7 (25%) still had no tumor regrowth by Day 14.

We measured the intratumoral NO concentration by microelectrode at various time points before and after treatment in this tumor model. The baseline MethA tumor NO concentration was 1.15 ± 0.05 μM (Fig. 2*a*). Following TNF, this rose to 1.85 ± 0.20 μM at 30 min ($p < 0.05$) and remained elevated until 3 hr, achieving a peak at 2.5 hr of 2.36 ± 0.24 μM (Fig. 2*a*). After 3 hr, the tumor NO concentration returned to baseline (Fig. 2*a*). There was no change in MethA tumor NO concentration after BSA injection (data not shown). The baseline LL2 tumor NO concentration was 1.60 ± 0.31 μM, and there was no appreciable change after TNF injection (Fig. 2*b*). Although the baseline NO concentration tended to be slightly higher in the LL2 tumors compared to MethA tumors, this difference was not statistically significant ($p = 0.2270$).

To evaluate the importance of NO in the antitumor response of TNF, we inhibited the production of NO in our experiments with low-dose 1400 W which selectively inhibits iNOS. We documented NO inhibition by microelectrode measurements and assessed the impact of NO inhibition on the antitumor effect of TNF. Pretreatment with low-dose 1400 W at selective iNOS inhibitory doses (5 mg/kg) 30 min prior to TNF completely blocked the rise in tumor NO concentration in MethA (Fig. 2*c*). Response rate decreased from 96% (27/28 MethA tumor bearing mice responded to TNF treatment in the control mice) to 38% (only 3/8 MethA tumor bearing mice responded to TNF when 1400 W was also administered) ($p = 0.0006$). Low-dose 1400 W had no effect on the response rate or the baseline NO levels in LL2 tumors after TNF (0% response rate in both groups); 1400 W at these doses resulted in no toxicity (data not shown).

Relative blood flow in both MethA and LL2 tumors decreased significantly by 4 hr after TNF (0.029 ± 0.018 and 0.022 ± 0.006, respectively; $p < 0.05$ *vs.* time 0 for both; Fig. 3*a*). The MethA tumors had no substantial recovery of blood flow at 24 hr (0.128 ± 0.046) or 10 days (0.051 ± 0.023, Fig. 3*a*). In contrast, the LL2 tumor blood flow recovered to 0.555 ± 0.360 at 24 hr after TNF and increased to 2.318 ± 0.958 above baseline by 10 d (Fig. 3*a*). The blood volume changes were similar to the blood flow changes; at 24 hr after TNF there was no substantial recovery in MethA (0.115 ± 0.045), whereas the relative blood volume in LL2 was 1.755 ± 1.592 (Fig. 3*b*). Ten days after TNF, blood volume in MethA was 0.107 ± 0.041, compared to 17.72 ± 14.40 in LL2 (Fig. 3*b*). As a control, MethA tumors were treated with BSA, and there was no significant change in blood flow or blood volume at 4 hr (0.95 ± 0.08 and 1.04 ±0.24, respectively; data not shown). Representative CD ultrasound images of MethA and LL2 tumors are shown in Figure 3*c*.

To confirm the vascular shutdown in the MethA tumors after TNF observed with Doppler ultrasound, we evaluated tumor

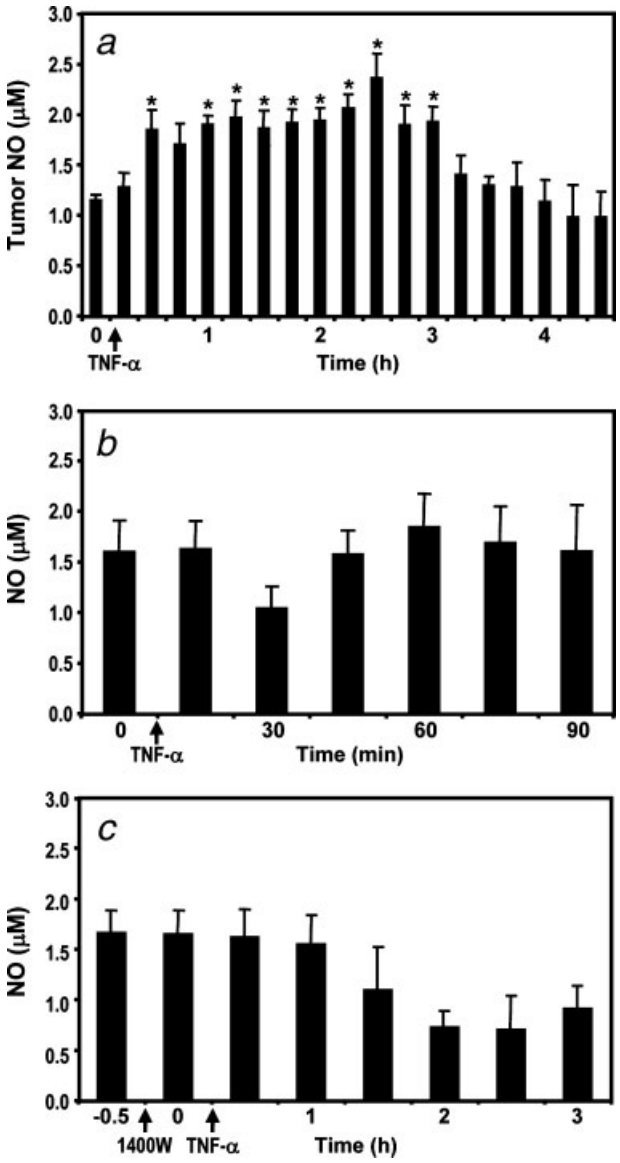

FIGURE 2 – Tumor NO concentration following TNF. (*a*). A single dose of TNF resulted in a significant increase in tumor NO concentration in MethA tumors by 30 min and this persisted until 3 hr. $*p < 0.05$ *vs.* baseline. Bars, SE. (*b*). There was no significant change in the LL2 tumor NO concentration following TNF. Bars, SE. (*c*) Pretreatment of MethA tumors with the low-dose (5 mg/kg) selective iNOS inhibitor 1400 W 30 min prior to TNF administration blocked the induction of tumor NO. Bars, SE.

perfusion with Hoechst dye injection after TNF. MethA tumor perfusion, analyzed by tumor uptake of Hoechst dye, was slightly decreased by 45 min after TNF, was minimal by 90 min, and was undetectable at 120 and 180 min (Fig. 4). This confirmed the blood flow shutdown seen with Doppler ultrasound and further delineated the time-course of this response.

Next the cell-type source for the NO burst post-TNF within the MethA tumor was explored. Tumor tissue cryosections from TNF- or BSA-treated MethA and LL2 tumors were immunohistochemically stained for iNOS at various time-points post-TNF treatment. MethA tumors showed spotted immunostaining for iNOS expression from about 30 min until 4-hr posttreatment, after which timepoint the tumor tissue showed visible signs of necrosis and no signs of iNOS expression (Fig. 5*c*). TNF-treated LL2 (Fig. 5*a*) and

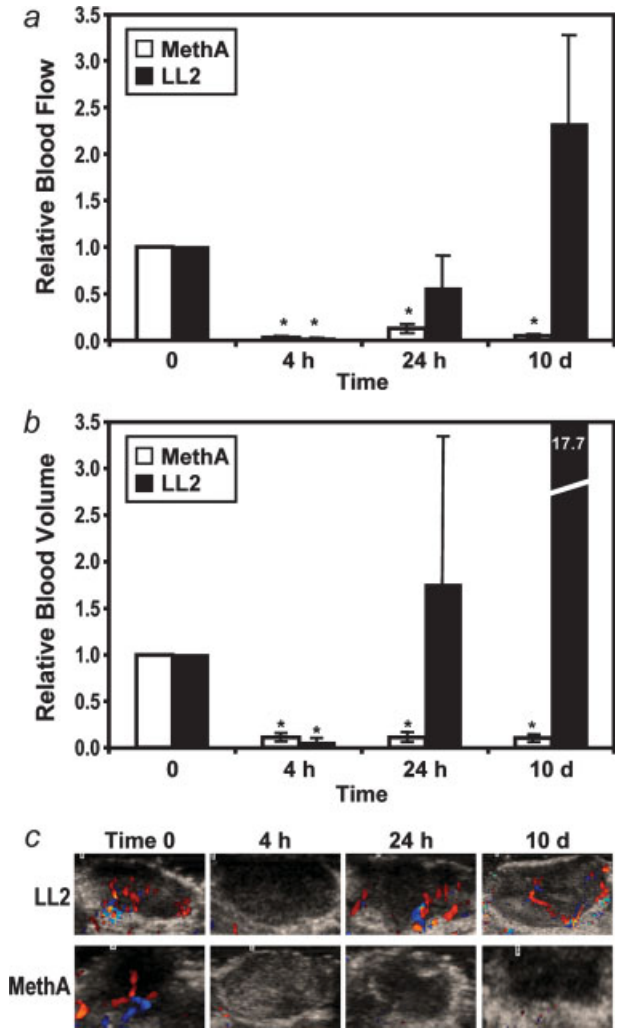

FIGURE 3 – Doppler ultrasound measurement of tumor blood flow and blood volume following TNF. (*a*) A single dose of TNF resulted in near complete cessation of tumor blood flow in MethA and LL2 tumors by 4 hr. LL2 tumors showed significant recovery of blood flow by 24 h, and a significant increase in blood flow at 10 days compared to baseline. MethA tumors exhibited no recovery of tumor blood flow at 24 hr or 10 days. $*p < 0.05$ *vs.* time 0. Bars, SE. (*b*) TNF led to a significant decrease in tumor blood volume in MethA tumors and LL2 tumors by 4 hr. LL2 tumors showed significant recovery of blood volume by 24 hr, and a significant increase in blood volume at 10 days compared to baseline. MethA tumors exhibited no recovery of tumor blood volume at 24 hr or 10 days. $*p < 0.05$ *vs.* time 0. Bars, SE. (*c*) Representative color Doppler images of tumor blood flow following TNF. [Color figure can be viewed in the online issue, which is available at www.interscience.wiley.com.]

BSA-treated MethA (Fig. 5*b*) and BSA-treated LL2 (data not shown) tumor tissue sections did not show any immunostaining for iNOS at any of the time-points studied. By microscopic examination of the immunostained tumor cryosections, it appeared that the cell-type source for iNOS was not tumor cells. In order to further investigate the cell-type source that was responsible for iNOS expression post-TNF, serial cryosections from both tumor types that were treated with TNF or BSA were immunohistochemically stained for macrophages. The localization of macrophage immunostaining appeared to mirror the immunostaining seen with iNOS in the MethA tumor cryosections (Fig. 5*f*). TNF-treated LL2 tumor cryosections (Fig. 5*d*) as well as BSA-treated MethA (Fig. 5*e*) and LL2 (data not shown) tumor cryosections did not show any immunostaining for macrophages. To confirm whether there was any overlap in localization of iNOS and macrophage immunostaining in TNF treated MethA tumor cryosections, double immunohistochemical staining for both iNOS and macrophages was performed on the same tumor tissue section. An exact overlap of immunohistochemical staining was observed with iNOS and macrophage specific antibodies in the MethA tumor type at 30-min, 1-, 2- and 4-hr post-TNF. Figure 5*g* represents the double-immunostained tumor tissue section at 4-hr post-TNF.

It was not clear at this point as to what role, if any, the tumor infiltrating macrophage-mediated iNOS played in tumor regression. To determine whether depletion of macrophages in BALB/c mice carrying MethA tumors would prevent the NO burst post-TNF and would make these tumors refractive to TNF, mice were treated with either 25 mg of silica in sterile PBS or 100 μl of clodronate-containing liposomes intraperitoneally 24 h before TNF treatment. Depletion of macrophages up to 4 days after silica/chlodronate treatment was confirmed by immunostaining of mouse liver and spleen cryosections for macrophages (data not shown). When such tumor-bearing mice were treated with TNF 24-hr postmacrophage depletion, tumor tissue sections did not show macrophage infiltration by immunohistochemical staining at 30-min, 1-, 2- or 4-hr post-TNF (Figs. 6*b* and 6*c*). Also, while tumor NO levels measured using a recessed probe microelectrode remained at or dropped below baseline levels in macrophage-depleted MethA tumors, tumor NO values escalated in relation to pretreatment values as expected in nondepleted tumors at 30 min (150 ± 20% of baseline), 60 min (180 ± 30% of baseline), and 90 min (225 ± 50% of baseline) ($p < 0.05$) post-TNF treatment (Fig. 7). Most significantly, macrophage depleted tumors failed to necrose, indicating that tumor infiltration by macrophages may be a prerequisite for MethA tumor ulceration post-TNF (Fig. 8). Control tumors in nonmacrophage depleted BALB/c mice necrosed in response to TNF treatment as expected (Fig. 8).

In order to determine whether macrophages activated by TNF could be cytotoxic to MethA tumor cells in culture, macrophages isolated from thiogylcollate exposed mice and activated with TNF were coincubated with radiolabeled MethA cells *in vitro*. Data obtained showed that tumor cells exposed to activated (TNF-exposed) macrophages showed maximum release of tritiated thymidine (33.4 ± 12.6%) when compared with tumor cells that were exposed to nonactivated macrophages (14 ± 2%; $p < 0.01$) or control tumor cells that were not exposed to macrophages (8.1 ± 0; $p < 0.001$; Fig. 9). The above data suggest that once tumors have been infiltrated by activated macrophages, they are sufficient to produce tumor cell kill.

To determine whether MethA and LL2 tumor cells were equally susceptible to physiologically relevant pathological quantities of NO in an *in vitro* setting, tumor cells were exposed to various concentrations ranging from 0 to 800 μM SNAP so as to produce physiologically relevant pathological amounts of NO. No significant cytotoxicity was observed in either tumor cell type after incubations with concentrations of SNAP less than 100 μM. Between 100 and 800 μM concentrations of SNAP exposure, both MethA and LL2 tumor cells showed equivalent susceptibility to NO (Fig. 10), further suggesting that the differential infiltration of the 2 tumor types by macrophages is the limiting factor in producing tumor cell kill.

To test whether TNF could differentially impact transit of monocytes exposed to MethA or LL2 tumor conditioned medium, mouse monocytes were exposed to MethA or LL2 conditioned medium with or without TNF and the migration of cell/hpf was recorded. Transit of monocytes in response to TNF (mean ± SD) averaged 94 ± 19 cells/hpf for LL2 medium, 120 ± 31/hpf for TNF-LL2 medium, 97 ± 39 cells/hpf for MethA medium, 121 ± 48/hpf for TNF-MethA medium. This compared to 49 ± 21 cells/hpf for RPMI alone, 49 ± 29 cells for TNF-RPMI, and 100 ± 37 cells/hpf for fMLP. When adjusted for random migration, (monocytes counted in RPMI alone), transit averaged 46 ± 12cells/hpf for LL2, 71 ± 13 cells/hpf for TNF-LL2, 49 ± 15 cells/hpf for

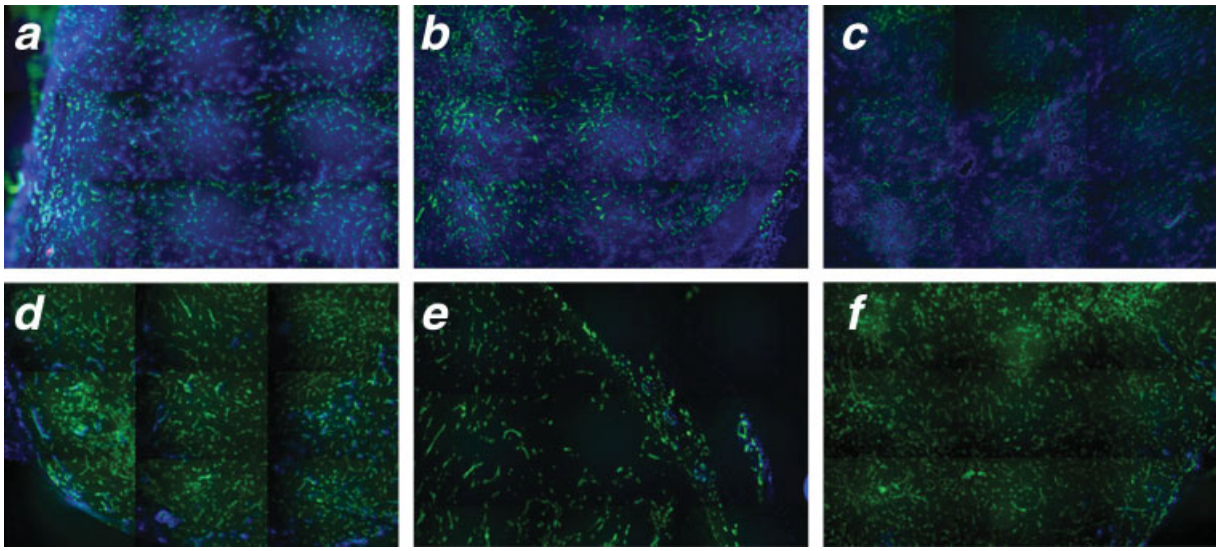

Figure 4 – Tumor perfusion in MethA following TNF. Tumor uptake of Hoechst dye (blue staining) was measured to assess tumor perfusion following treatment with TNF. Tumor perfusion was slightly decreased by 45 min, was minimal by 90 min, and was undetectable at 120 min and 180 min. (*a*), 30 min; (*b*) 45 min; (*c*) 60 min; (*d*) 90 min; (*e*) 120 min; (*f*) 180 min. [Color figure can be viewed in the online issue, which is available at www.interscience.wiley.com.]

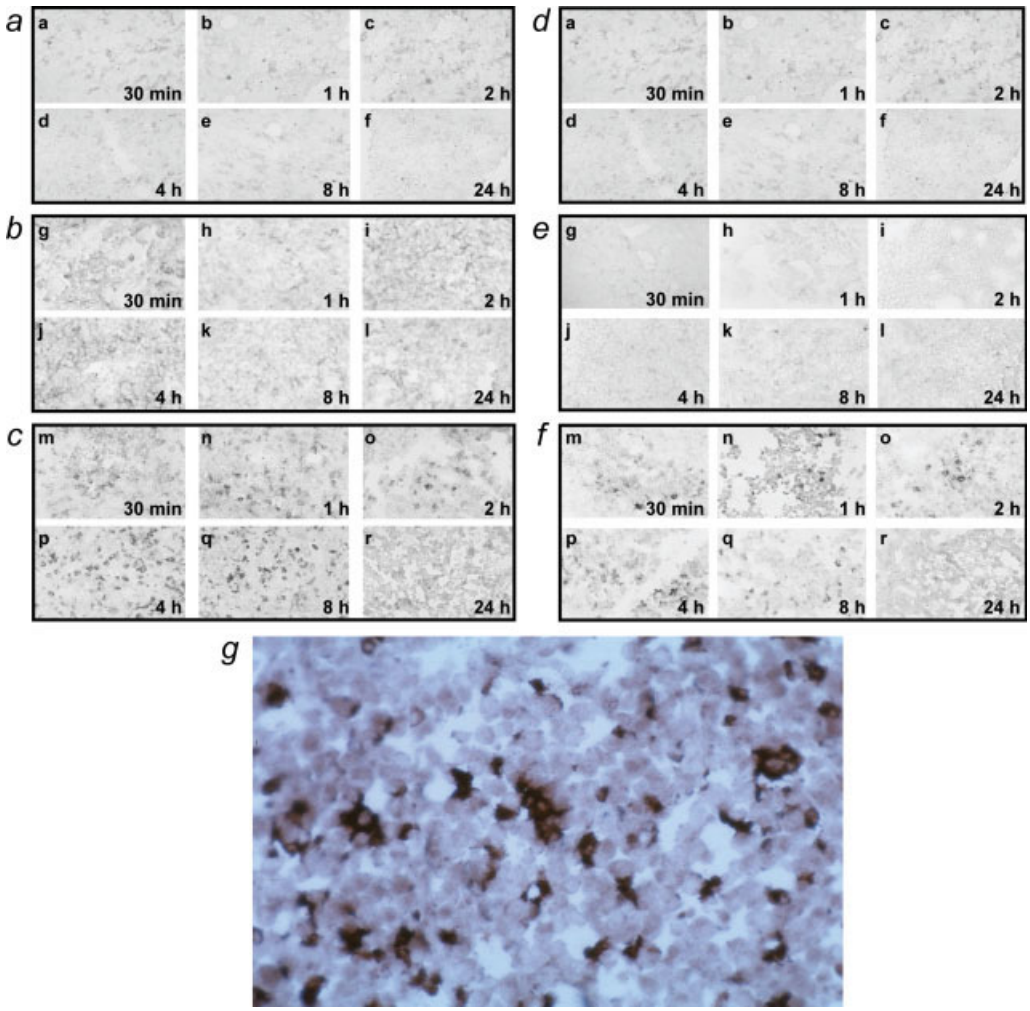

Figure 5 – Immunohistochemical staining for iNOS (*a*, *b* and *c*) and for macrophages (*d*, *e*, and *f*) of MethA and LL2 tumor cryosections and double immunohistochemical staining for iNOS and macrophages in TNF-treated MethA tumor (*g*). TNF-treated LL2 (*a*, *d*) and BSA-treated MethA (*b*, *e*) tumors did not show any immunostaining for iNOS or macrophages. TNF-treated MethA tumors show immunostaining for both iNOS (*c*) as well as for macrophages (*f*). Double immunostaining showed that iNOS localizes to macrophages in TNF-treated MethA tumors (*g*). [Color figure can be viewed in the online issue, which is available at www.interscience.wiley.com.]

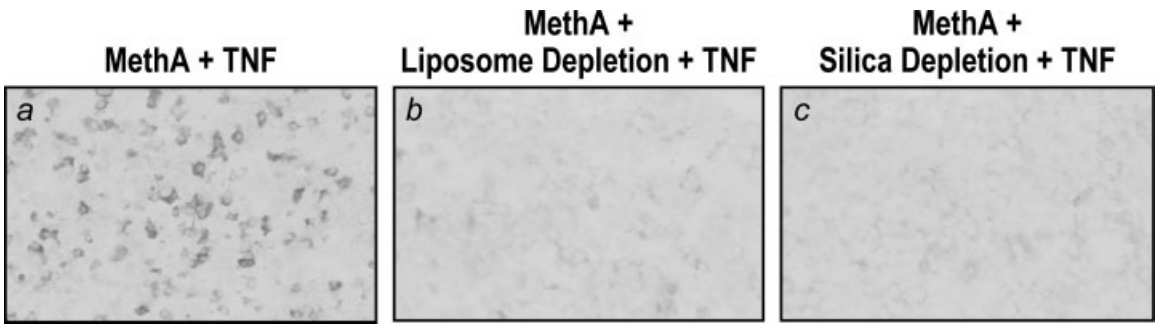

FIGURE 6 – Immunohistochemical staining for macrophages before and after depletion in tumor cryosections. MethA tumor cryosection at 4 hr after TNF-treatment (*a*) showing macrophage infiltration while at 4 hr after TNF treatment in postmacrophage-depleted tumors (*b* and *c*) showing no macrophages.

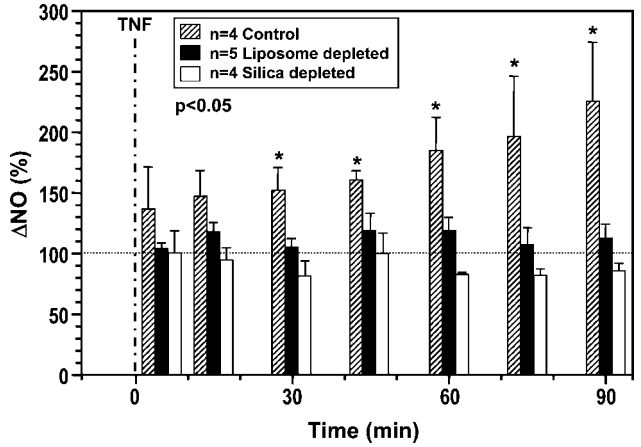

FIGURE 7 – Tumor NO levels measured before and after macrophage depletion using a recessed probe microelectrode. NO levels remained at or dropped below baseline levels in macrophage-depleted MethA tumors, while tumor NO values escalated in relation to pretreatment values as expected in nondepleted tumors at 30 min (150 ± 20% of baseline), 60 min (180 ± 30% of baseline) and 90 min (225 ± 50% of baseline; $p < 0.05$) post-TNF treatment.

MethA, 69 ± 18 cells/hpf for TNF-MethA. Results are summarized in Figure 11. The statistical test for trend for the different conditioned media was significant at $p = 0.043$. The 1-way analysis of variance that tested whether the mean migration was different between the different conditioned media was significant at $p = 0.0012$. To test for specific differences between groups, a 1-way pairwise analysis of variance was carried out with Bonferroni correction for multiple testing. Data showed that while there was no difference between LL2 *versus* MethA, LL2-TNF *versus* MethA-TNF or RPMI *versus* RPMI-TNF directed monocyte migration ($p = 1.0$ in all instances), there was significant difference between the RPMI/RPMI-TNF group *versus* MethA-TNF ($p = 0.015$) or LL2-TNF ($p = 0.017$) groups. These analyses suggest that while there was no difference between the movement of monocytes in response to MethA-TNF conditioned medium and that in response to LL2-TNF conditioned medium, this migration is likely not random and could be a result of chemotaxis in response to TNF tumor conditioned medium.

To determine what molecules could be responsible for selective tumor infiltration of macrophages between MethA and LL2 tumors, TNF-treated MethA or LL2 tumor cells were analyzed for expression of the chemokine, monocyte chemotactic protein (MCP-1) by ELISA at 1- or 2-hr posttreatment at varying concentrations of TNF. Data indicate that both MethA and LL2 tumor cells produced equivalent amounts of MCP-1 at the different concentrations of TNF used and at the different time-points studied (data not shown).

Furthermore, since upregulation of cell adhesion molecules that line the vasculature (ICAM, VCAM and E-selectin) have been implicated in extravasation of monocytes to extracellular sites, the level of expression was measured in the 2 tumor cell lines before and after TNF treatment by immunohistochemical methods as well as by ELISA at 1-, 2-and 4-hr post-TNF treatment. While VCAM and E-selectin showed no differences in level of expression in MethA and LL2 tumors pre- and/or post-TNF treatment, ICAM expression was moderately more pronounced in MethA when compared with LL2 tumors as detected both by immunohistochemistry as well as by ELISA (data not shown).

Discussion

TNF is believed to cause tumor ulceration primarily *via* an antivascular effect specific to the tumor microenvironment.[15–18] However, the molecular mediators of this antivascular effect have not been delineated. There is limited data on the role of NO and the interaction between NO and tumor blood flow following TNF administration. In the present study, the role of NO and changes in tumor blood flow in TNF-mediated tumor regression were investigated.

Most studies on NO have employed techniques that measure NO indirectly *via* serum nitrate/nitrite analysis, rather than *via* direct real-time tumor measurement. Additionally, the lack of a reliable, repeatable and noninvasive method of measuring tumor blood flow and blood volume has limited progress in this field. Recently, direct measurements of tumor tissue NO have been reported by Kashiwagi *et al.*,[39] using the recessed NO microprobe as well as nonquantitative optical NO measurements. NO was shown to play a critical role in mural cell recruitment for angiogenesis, with the highest levels of NO measured in tumors with the greatest angiogenic activity. The baseline NO levels measured in our study were at the lower range of those reported by Kashiwagi *et al.*[39] The use of the recessed NO microprobe and Doppler ultrasound blood flow and blood volume measurement in our study contributed greatly to a quantitative investigation of the vascular effect of TNF on tumors.

The MethA and LL2 tumors had the same growth rate as evidenced by the BSA-treated control groups. In addition, there was no significant difference in baseline tumor NO concentration in the 2 tumors. The MethA tumors had a significant ulcerative response to TNF, easily measurable in the subcutaneous location, while the LL2 tumors reliably had no ulceration or growth suppression, making this an ideal model for this study.

TNF led to no increase in the LL2 NO concentration and resulted in no tumor responses, with a tumor growth curve similar

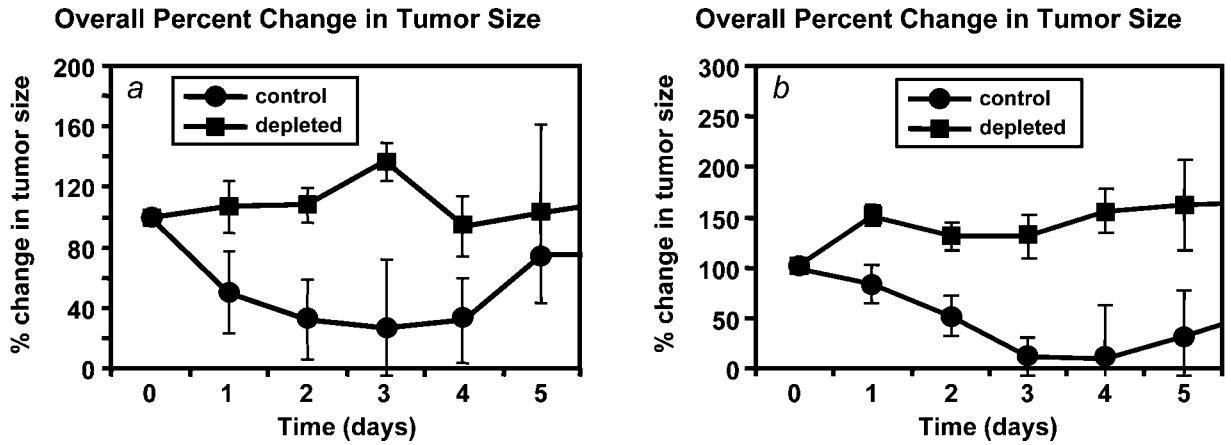

FIGURE 8 – Clinical tumor response to TNF in macrophage depleted (●) and control (■) mice using silica (*a*) and chlodronate containing liposomes (*b*). Control mice carrying MethA tumors show response to TNF while macrophage-depleted mice do not.

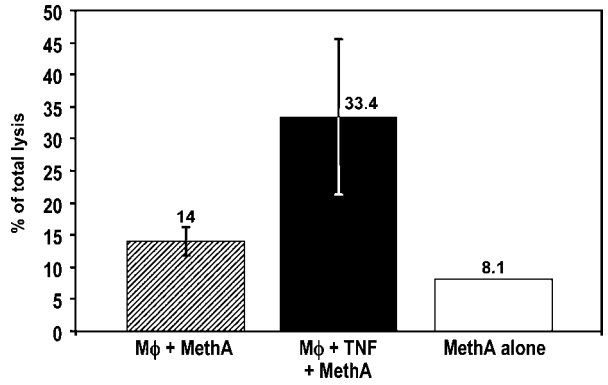

FIGURE 9 – *In vitro* experiment showing cytotoxicty of activated macrophages on tumor cells. Tumor cells exposed to activated (TNF-exposed) macrophages showed maximum release of tritiated thymidine (33.4 ± 12.6%) when compared with tumor cells that were exposed to nonactivated macrophages (14 ± 2%; $p < 0.01$) or control tumor cells that were not exposed to macrophages (8.1; $p < 0.001$).

to that of the BSA control group. However, blood flow and blood volume in LL2 was nearly completely inhibited by 4 hr. By 24 hr the relative blood flow had recovered substantially and by 10 days, it was greater than twice the baseline level. These data suggest that blood flow shutdown occurs even in nonulcerating tumors after TNF, but in the LL2 tumor this is temporary and recoverable and not due to clot. Additionally, this demonstrates that temporary blood flow shutdown alone is insufficient to cause tumor ulceration.

The NO concentration in the MethA tumors rose significantly to cytotoxic levels (>1.0–1.5 μM)[40,41] by 30 min and this response was sustained out to 3 hr with a maximum NO concentration of 2.36 ± 0.24 μM at 2.5 hr. The blood flow and blood volume were nearly completely inhibited by 4 hr. However, there was no recovery of blood flow or blood volume at 24 hr or 10 days, resulting in the significant necrosis and response seen in this tumor line. This blood flow shutdown was confirmed by Hoechst dye injection—decrease in blood flow started by 45 min and was nearly complete by 2 hr. We can conclude from these data that the addition of the NO burst to blood flow shutdown results in tumor necrosis with permanent loss of tumor blood flow.

The NOS inhibitor experiments were carried out to delineate the role of iNOS in tumor NO elevation, tumor ulceration and blood flow recovery after TNF. At selective iNOS inhibitory doses (5 mg/kg),[33] 1400 W given 30 min before TNF successfully blocked the rise in tumor NO and significantly lowered the response rate in MethA from 96 to 38% ($p = 0.006$). This demonstrates that TNF causes an iNOS-mediated increase in tumor NO, which is partly responsible for tumor ulceration.

In an attempt to determine the cell type source within the tumor for the NO burst post-TNF in the TNF-responsive tumor type, the present work initially used single color immunohistochemical analysis of TNF- or BSA-treated MethA and LL2 tumor cryosections using antibodies for iNOS and found that only TNF-treated MethA tumor cryosections from 30 min to 4-hr post-TNF showed positive spotty immunostaining for iNOS. Furthermore, it was evident that iNOS immunostaining was localized to cells other than tumor cells, and additional single and double immunohistochemical analyses revealed that there was an exact overlap between iNOS expression and localization of tumor-infiltrating macrophages. Other investigators have shown that ILP with TNF can cause tumor infiltration by macrophages as well.[42] LL2 tumor cryosections as well as BSA-treated MethA and LL2 tumor tissue sections did not show any immunostaining for iNOS or macrophages. Thus, the cell-type source of the NO burst post-TNF was determined to be tumor infiltrating macrophages in the responsive MethA tumor. Other studies have also shown that leukocytes play an important role in the hemorrhagic effects of TNF.[43]

To further delineate the role of macrophage-derived iNOS in TNF-mediated tumor regression, monocytes were depleted in MethA tumor bearing BALB/c mice by intraperitoneal injections of silica in PBS or clodronate containing liposomes. Depleted mice did not show positive immunostaining for macrophages in their spleens, liver or tumors as late as 4 days posttreatment with the macrophage depleting agents. Such tumor-bearing mice were then treated with TNF 24 hr after macrophage depletion, and data obtained showed that depletion of tumor macrophages prevented production of NO post-TNF in the responsive tumor. Also tumor regression post-TNF was fully inhibited in these mice, and tumors continued to grow at a rate comparable to nondepleted, non-TNF treated tumors. Taken together, the earlier set of experiments suggested that there is possibly a second component to the tumoricidal activity of TNF, one apart from the vasculature-mediated indirect tumor cell kill. This second component appears to be macrophage-derived NO-mediated tumor cell kill. Work from other laboratories has shown that leukocytes, in general, play an important role in the antitumor response of TNF.[44] Another study has shown a decrease in numbers of monocytes in the circulation after TNF treatment. The same study also showed increased mononuclear cell-derived *in vitro* cytokine production after TNF treatment.[45]

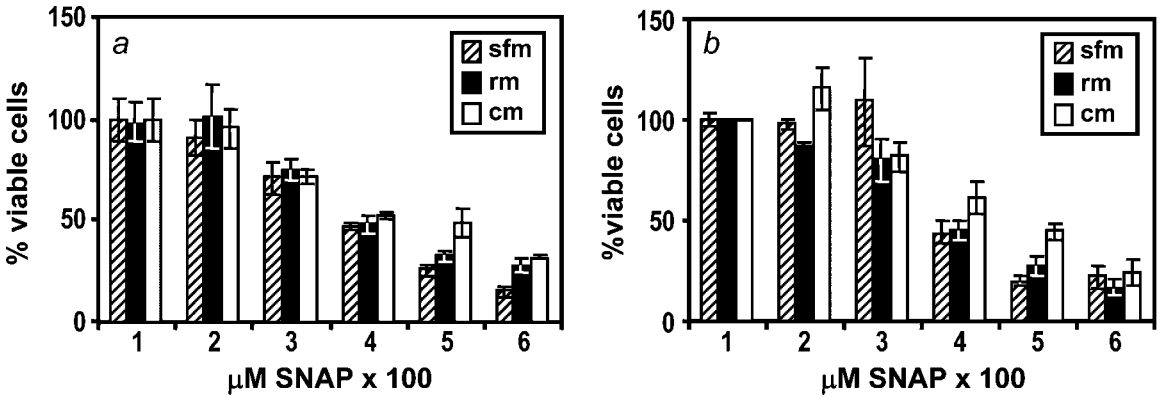

FIGURE 10 – *In vitro* experiment showing equal susceptibility of MethA cells (*a*) and LL2 cells (*b*) to NO.

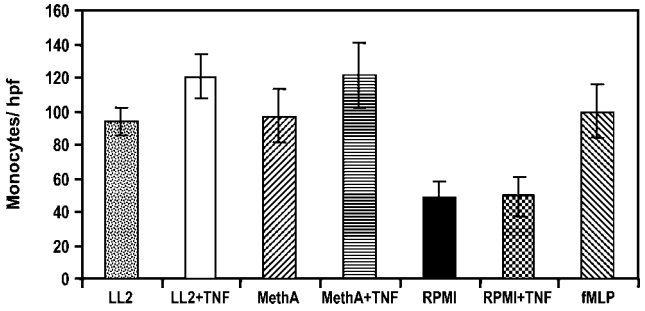

FIGURE 11 – *In vitro* experiment showing movement of monocytes in response to TNF-exposed MethA or LL2 conditioned culture medium. Transit of monocytes averaged 94 ± 19cells/hpf for LL2 medium, 120 ± 31/hpf for TNF-LL2 medium, 97 ± 39 cells/hpf for MethA medium, 121 ± 48/hpf for TNF-MethA medium. This compared to 49 ± 21 cells/hpf for RPMI alone, 49 ± 29 cells for TNF-RPMI and 100 ± 37 cells/hpf for fMLP. When adjusted for random migration, (monocytes counted in RPMI alone), transit averaged 46 ± 12cells/hpf for LL2, 71 ± 13 cells/hpf for TNF-LL2, 49 ± 15 cells/hpf for MethA and 69 ± 18 cells/hpf for TNF-MethA.

In the next set of experiments, we observed in an *in vitro* setting that macrophages isolated from the peritoneum of BALB/c mice and activated *ex vivo* with TNF were equally cytotoxic to both MethA and LL2 cells in culture. Also, both MethA and LL2 cells were equally susceptible to the NO donor SNAP in an *in vitro* cell culture setting at physiologically relevant pathological quantities of NO. Taken together, the earlier set of experiments suggest that while both tumor types are equally susceptible to the cytotoxic effects of TNF-induced macrophage-mediated NO release, what determines whether a tumor is sensitive or resistant to TNF is the sequence of events that lead to tumor infiltration by macrophages in the TNF-sensitive tumor type and its absence in the TNF-resistant tumor type.

Another question that the present work attempts to address is the molecular mechanism underlying the tumor-type dependent response to TNF. In the model used in this work, the MethA fibrosarcoma is responsive to TNF while the LL2 tumor is resistant to TNF. In an effort to determine what specific factors expressed differentially or acting differently in the 2 tumor types could contribute to the TNF sensitive/resistant phenotype as in the case of the MethA-LL2 tumor systems, we looked at the expression levels of cell-adhesion molecules on the surface of the vasculature in the 2 tumor types. Specifically, we looked at the expression of ICAM, VACM and E-selectin in the vasculatures of MethA and LL2 tumors and found no significant differences in the expression patterns or levels of these molecules in the 2 tumor types. This observation departs from other studies that have shown differences in 1 or more of these cell adhesion molecules.[46,47] Furthermore, we looked at the expression of MCP-1 in the MethA and LL2 tumors and found no significant differences in the expression of this molecule pre- and post-TNF treatment between the 2 tumor types.

Other investigators have looked at alternative molecules that could potentially mediate an enhanced antitumor response to ILP with TNF. One such candidate molecule is the endothelial monocyte-activating polypeptide II (EMAP-II), which is a tumor-derived cytokine. Its expression appears to increase the TNF receptor on tumor endothelium, and enhance the induction of tissue factor on endothelial cells, resulting in an antiangiogenic effect. It has been shown that *in vivo* sensitivity of the tumor vasculature to TNF is determined by the tumor production of EMAP-II.[48–50] This work also showed that EMAP-II is produced in various levels and that one can increase the sensitivity of tumor to TNF therapy *in vivo* by upregulating EMAP-II production. Apart from being an antiangiogenic molecule, EMAP-II is also a modulator of inflammatory reactions. Under pathophysiological conditions, EMAP-II appears to have several functions. It is known to trigger the recruitment of macrophages by elevating cytosolic-free Ca^{2+} concentrations, it stimulates leukocyte chemotaxis, induces the expression of endogenous TNF-α and tissue factor by monocytes and myeloperoxidase by polymorphonuclear cells. Another study concluded that quantifiable differences in the hyperpermeability of the tumor vasculature and the extent of the tumor vasculature that is sensitive to TNF is the basis for the differential response of distinct tumor types to TNF.[42] The earlier 2 observations could plausibly hold the key to the differential response of MethA and LL2 tumor types to TNF treatment. This question is currently under investigation.

In another study carried out on 19 patients with locally advanced soft tissue sarcoma solid tumors, TNF-α induced the expression of an RNA binding protein (TIA-1) with translation-regulatory properties that not only had the potential to sensitize endothelial cells that are in the tumor microenvironment to proapoptotic stimuli and also to enhance NK cell cytotoxic activity.[51]

We have demonstrated that TNF causes tumor ulceration *via* a tumor-infiltrating macrophage-derived iNOS-mediated tumor NO burst combined with a blood flow shutdown in the TNF-responsive tumor, MethA. Temporary blood flow shutdown is insufficient to cause tumor ulceration as seen in the case of the LL2 tumor post-TNF. It needs to be sustained through 4 hr and 10 days post-TNF, as seen in the case of the MethA tumor type. This study has also shown that the limiting factor in tumor response to TNF is tumor infiltration by macrophages immediately after exposure to TNF. A more complete understanding of the downstream molecular pathways initiated by high-dose TNF treatment leading to tumor ulceration including tumor NO and tumor blood flow changes may aid in the development of novel vascular-targeted therapies.

References

1. Hurwitz H, Fehrenbacher L, Novotny W, Cartwright T, Hainsworth J, Heim W, Berlin J, Baron A, Griffing S, Holmgren E, Ferrara N, Fyfe G, et al. Bevacizumab plus irinotecan, fluorouracil, and leucovorin for metastatic colorectal cancer. N Engl J Med 2004;350:2335–42.
2. Hicklin DJ, Ellis LM. Role of the vascular endothelial growth factor pathway in tumor growth and angiogenesis. J Clin Oncol 2005;23: 1011–27.
3. Siemann DW, Bibby MC, Dark GG, Dicker AP, Eskens FA, Horsman MR, Marme D, Lorusso PM. Differentiation and definition of vascular-targeted therapies. Clin Cancer Res 2005;11:416–20.
4. Lienard D, Ewalenko P, Delmotte JJ, Renard N, Lejeune FJ. High-dose recombinant tumor necrosis factor alpha in combination with interferon gamma and melphalan in isolation perfusion of the limbs for melanoma and sarcoma. J Clin Oncol 1992;10:52–60.
5. Lienard D, Eggermont AM, Kroon BB, Schraffordt Koops H, Lejeune FJ. Isolated limb perfusion in primary and recurrent melanoma: indications and results. Semin Surg Oncol 1998;14:202–9.
6. Fraker DL, Alexander HR, Andrich M, Rosenberg SA. Treatment of patients with melanoma of the extremity using hyperthermic isolated limb perfusion with melphalan, tumor necrosis factor, and interferon gamma: results of a tumor necrosis factor dose-escalation study. J Clin Oncol 1996;14:479–89.
7. Fraker DL, Alexander HR. Isolated limb perfusion with high-dose tumor necrosis factor for extremity melanoma and sarcoma. In: DeVita V, Hellman S, Rosenberg SA, eds. Important Advances in Oncology. Philadelphia: Lippincott, 1994:179–92.
8. Alexander HR Jr, Fraker DL, Bartlett DL. Isolated limb perfusion for malignant melanoma. Semin Surg Oncol 1996;12:416–28.
9. Grover A, Alexander HR Jr. The past decade of experience with isolated hepatic perfusion. Oncologist 2004;9:653–64.
10. Eggermont AM, ten Hagen TL. Isolated limb perfusion for extremity soft-tissue sarcomas, in-transit metastases, and other unresectable tumors: credits, debits, and future perspectives. Curr Oncol Rep 2001; 3:359–67.
11. Fraker DL. Hyperthermic regional perfusion for melanoma and sarcoma of the limbs. Curr Probl Surg 1999;36:841–907.
12. Noorda EM, Vrouenraets BC, Nieweg OE, van Geel AN, Eggermont AM, Kroon BB. Safety and efficacy of isolated limb perfusion in elderly melanoma patients. Ann Surg Oncol 2002;9:968–74.
13. Takkenberg RB, Vrouenraets BC, van Geel AN, Nieweg OE, Noorda EM, Eggermont AM, Kroon BB. Palliative isolated limb perfusion for advanced limb disease in stage IV melanoma patients. J Surg Oncol 2005;91:107–11.
14. Alexander HR, Jr, Bartlett DL, Libutti SK. Current status of isolated hepatic perfusion with or without tumor necrosis factor for the treatment of unresectable cancers confined to liver. Oncologist 2000;5: 416–24.
15. Manda T, Shimomura K, Mukumoto S, Kobayashi K, Mizota T, Hirai O, Matsumoto S, Oku T, Nishigaki F, Mori J, Hiroyuki K. Recombinant human tumor necrosis factor-alpha: evidence of an indirect mode of antitumor activity. Cancer Res 1987;47:3707–11.
16. Nawroth P, Handley D, Matsueda G, De Waal R, Gerlach H, Blohm D, Stern D. Tumor necrosis factor/cachectin-induced intravascular fibrin formation in meth A fibrosarcomas. J Exp Med 1988;168:637–47.
17. Watanabe N, Niitsu Y, Umeno H, Kuriyama H, Neda H, Yamauchi N, Maeda M, Urushizaki I. Toxic effect of tumor necrosis factor on tumor vasculature in mice. Cancer Res 1988;48:2179–83.
18. Kallinowski F, Schaefer C, Tyler G, Vaupel P. In vivo targets of recombinant human tumour necrosis factor-alpha: blood flow, oxygen consumption and growth of isotransplanted rat tumours. Br J Cancer 1989;60:555–60.
19. Busse R, Mulsch A. Induction of nitric oxide synthase by cytokines in vascular smooth muscle cells. FEBS Lett 1990;275:87–90.
20. Cambien B, Bergmeier W, Saffaripour S, Mitchell HA, Wagner DD. Antithrombotic activity of TNF-alpha. J Clin Invest 2003;112:1589–96.
21. Kilbourn RG, Belloni P. Endothelial cell production of nitrogen oxides in response to interferon gamma in combination with tumor necrosis factor, interleukin-1, or endotoxin. J Natl Cancer Inst 1990; 82:772–6.
22. Lamas S, Michel T, Brenner BM, Marsden PA. Nitric oxide synthesis in endothelial cells: evidence for a pathway inducible by TNF-alpha. Am J Physiol 1991;261:C634–41.
23. Liew FY, Li Y, Millott S. Tumor necrosis factor-alpha synergizes with IFN-gamma in mediating killing of Leishmania major through the induction of nitric oxide. J Immunol 1990;145:4306–10.
24. Gaillard T, Mulsch A, Busse R, Klein H, Decker K. Regulation of nitric oxide production by stimulated rat Kupffer cells. Pathobiology 1991;59:280–3.
25. Xie K, Huang S, Dong Z, Juang SH, Gutman M, Xie QW, Nathan C, Fidler IJ. Transfection with the inducible nitric oxide synthase gene suppresses tumorigenicity and abrogates metastasis by K-1735 murine melanoma cells. J Exp Med 1995;181:1333–43.
26. Xie K, Dong Z, Fidler IJ. Activation of nitric oxide synthase gene for inhibition of cancer metastasis. J Leukoc Biol 1996;59:797–803.
27. Jyothi MD, Khar A. Induction of nitric oxide production by natural killer cells: its role in tumor cell death. Nitric Oxide 1999;3:409–18.
28. Shinohara H, Bucana CD, Killion JJ, Fidler IJ. Intensified regression of colon cancer liver metastases in mice treated with irinotecan and the immunomodulator JBT 3002. J Immunother 2000;23:321–31.
29. Kelley ST, Menon C, Buerk DG, Bauer TW, Fraker DL. Acidosis plus melphalan induces nitric oxide-mediated tumor regression in an isolated limb perfusion human melanoma xenograft model. Surgery 2002;132:252–8.
30. Millet A, Bettaieb A, Renaud F, Prevotat L, Hammann A, Solary E, Mignotte B, Jeannin JF. Influence of the nitric oxide donor glyceryl trinitrate on apoptotic pathways in human colon cancer cells. Gastroenterology 2002;123:235–46.
31. Li LM, Kilbourn RG, Adams J, Fidler IJ. Role of nitric oxide in lysis of tumor cells by cytokine-activated endothelial cells. Cancer Res 1991;51:2531–5.
32. Carmichael J, DeGraff WG, Gazdar AF, Minna JD, Mitchell JB. Evaluation of a tetrazolium-based semiautomated colorimetric assay: assessment of radiosensitivity. Cancer Res 1987;47:943–6.
33. Garvey EP, Oplinger JA, Furfine ES, Kiff RJ, Laszlo F, Whittle BJ, Knowles RG. 1400W is a slow, tight binding, and highly selective inhibitor of inducible nitric-oxide synthase in vitro and in vivo. J Biol Chem 1997;272:4959–63.
34. Buerk DG, Riva CE, Cranstoun SD. Nitric oxide has a vasodilatory role in cat optic nerve head during flicker stimuli. Microvasc Res 1996;52:13–26.
35. Sehgal CM, Arger PH, Rowling SE, Conant EF, Reynolds C, Patton JA Quantitative vascularity of breast masses by Doppler imaging: regional variations and diagnostic implications. J Ultrasound Med 2000;19:427–40; quiz 441–2.
36. Menon C, Polin GM, Prabakaran I, Hsi A, Cheung C, Culver JP, Pingpank JF, Sehgal CS, Yodh AG, Buerk DG, Fraker DL. An integrated approach to measuring tumor oxygen status using human melanoma xenografts as a model. Cancer Res 2003;63:7232–40.
37. Chaplin DJ, Olive PL, Durand RE. Intermittent blood flow in a murine tumor: radiobiological effects. Cancer Res 1987;47:597–601.
38. Arndt-Jovin DJ, Jovin TM. Analysis and sorting of living cells according to deoxyribonucleic acid content. J Histochem Cytochem 1977;25:585–9.
39. Kashiwagi S, Izumi Y, Gohongi T, Demou ZN, Xu L, Huang PL, Buerk DG, Munn LL, Jain RK, Fukumura D. NO mediates mural cell recruitment and vessel morphogenesis in murine melanomas and tissue-engineered blood vessels. J Clin Invest 2005;115:1816–27.
40. Knowles RG. Nitric oxide biochemistry. Biochem Soc Trans 1997;25: 895–901.
41. Murphy MP. Nitric oxide and cell death. Biochim Biophys Acta 1999;1411:401–14.
42. Nooijen PT, Eggermont AM, Schalkwijk L, Henzen-Logmans S, de Waal RM, Ruiter DJ. Complete response of melanoma-in-transit metastasis after isolated limb perfusion with tumor necrosis factor alpha and melphalan without massive tumor necrosis: a clinical and histopathological study of the delayed-type reaction pattern. Cancer Res 1998;58:4880–7.
43. Manusama ER, Nooijen PT, Stavast J, de Wilt JH, Marquet RL, Eggermont AM. Assessment of the role of neutrophils on the antitumor effect of TNFalpha in an in vivo isolated limb perfusion model in sarcoma-bearing brown Norway rats. J Surg Res 1998;78: 169–75.
44. Renard N, Lienard D, Lespagnard L, Eggermont A, Heimann R, Lejeune F. Early endothelium activation and polymorphonuclear cell invasion precede specific necrosis of human melanoma and sarcoma treated by intravascular high-dose tumour necrosis factor alpha (rTNF alpha). Int J Cancer 1994;57:656–63.
45. Stam TC, Jongen-Lavrencic M, Eggermont AM, Swaak AJ. Effects of isolated limb perfusion with tumour necrosis factor-alpha on the function of monocytes and T lymphocytes in patients with cancer. Eur J Clin Invest 1996;26:1085–91.
46. Ferroni P, Di Filippo F, Martini F, Spila A, D'Alessandro T, Cavaliere F, Anza M, Garinei R, Aloe S, Carone MD, Gazzaniga PP, Guadagni F. Effects of isolated limb perfusion with tumor necrosis factor-alpha on circulating levels of proinflammatory cytokines. J Immunother 2001;24:354–62.
47. Nooijen PT, Eggermont AM, Verbeek MM, Schalkwijk L, Buurman WA, de Waal RM, Ruiter DJ. Transient induction of E-selectin

expression following TNF alpha-based isolated limb perfusion in melanoma and sarcoma patients is not tumor specific. J Immunother Emphasis Tumor Immunol 1996;19:33–44.
48. Kayton ML, Libutti SK. Endothelial monocyte activating polypeptide II (EMAP II) enhances the effect of TNF on tumor-associated vasculature. Curr Opin Investig Drugs 2001;2:136–8.
49. Lans TE, ten Hagen TL, van Horssen R, Wu PC, van Tiel ST, Libutti SK, Alexander HR, Eggermont AM. Improved antitumor response to isolated limb perfusion with tumor necrosis factor after upregulation of endothelial monocyte-activating polypeptide II in soft tissue sarcoma. Ann Surg Oncol 2002;9: 812–19.
50. Lans TE, van Horssen R, Eggermont AM, ten Hagen TL. Involvement of endothelial monocyte activating polypeptide II in tumor necrosis factor-alpha-based anti-cancer therapy. Anticancer Res 2004;24: 2243–8.
51. Mocellin S, Provenzano M, Lise M, Nitti D, Rossi CR. Increased TIA-1 gene expression in the tumor microenvironment after locoregional administration of tumor necrosis factor-alpha to patients with soft tissue limb sarcoma. Int J Cancer 2003;107:317–22.